Search for Bosonic Superweakly Interacting Massive Dark Matter Particles with the XMASS-I Detector

K. Abe,[1,2] K. Hieda,[1] K. Hiraide,[1,2] S. Hirano,[1] Y. Kishimoto,[1,2] K. Ichimura,[1,2] K. Kobayashi,[1,2] S. Moriyama,[1,2] K. Nakagawa,[1] M. Nakahata,[1,2] H. Ogawa,[1,2] N. Oka,[1] H. Sekiya,[1,2] A. Shinozaki,[1] Y. Suzuki,[1,2] A. Takeda,[1,2] O. Takachio,[1] D. Umemoto,[1] M. Yamashita,[1,2] B. S. Yang,[1,2] S. Tasaka,[3] J. Liu,[2] K. Martens,[2] K. Hosokawa,[4] K. Miuchi,[4] A. Murata,[4] Y. Onishi,[4] Y. Otsuka,[4] Y. Takeuchi,[4,2] Y. H. Kim,[5] K. B. Lee,[5] M. K. Lee,[5] J. S. Lee,[5] Y. Fukuda,[6] Y. Itow,[7,8] K. Masuda,[7] H. Takiya,[7] H. Uchida,[7] N. Y. Kim,[9] Y. D. Kim,[9] F. Kusaba,[10] K. Nishijima,[10] K. Fujii,[11] I. Murayama,[11] and S. Nakamura[11]

(XMASS Collaboration)

[1]*Kamioka Observatory, Institute for Cosmic Ray Research, the University of Tokyo, Higashi-Mozumi, Kamioka, Hida, Gifu 506-1205, Japan*
[2]*Kavli Institute for the Physics and Mathematics of the Universe (WPI), the University of Tokyo, Kashiwa, Chiba 277-8582, Japan*
[3]*Information and Multimedia Center, Gifu University, Gifu 501-1193, Japan*
[4]*Department of Physics, Kobe University, Kobe, Hyogo 657-8501, Japan*
[5]*Korea Research Institute of Standards and Science, Daejeon 305-340, South Korea*
[6]*Department of Physics, Miyagi University of Education, Sendai, Miyagi 980-0845, Japan*
[7]*Solar Terrestrial Environment Laboratory, Nagoya University, Nagoya, Aichi 464-8602, Japan*
[8]*Kobayashi-Masukawa Institute for the Origin of Particles and the Universe, Nagoya University, Furu-cho, Chikusa-ku, Nagoya, Aichi 464-8602, Japan*
[9]*Department of Physics, Sejong University, Seoul 143-747, South Korea*
[10]*Department of Physics, Tokai University, Hiratsuka, Kanagawa 259-1292, Japan*
[11]*Department of Physics, Faculty of Engineering, Yokohama National University, Yokohama, Kanagawa 240-8501, Japan*

(Received 1 June 2014; revised manuscript received 27 July 2014; published 18 September 2014)

Bosonic superweakly interacting massive particles (super-WIMPs) are a candidate for warm dark matter. With the absorption of such a boson by a xenon atom, these dark matter candidates would deposit an energy equivalent to their rest mass in the detector. This is the first direct detection experiment exploring the vector super-WIMPs in the mass range between 40 and 120 keV. With the use of 165.9 day of data, no significant excess above background was observed in the fiducial mass of 41 kg. The present limit for the vector super-WIMPs excludes the possibility that such particles constitute all of dark matter. The absence of a signal also provides the most stringent direct constraint on the coupling constant of pseudoscalar super-WIMPs to electrons. The unprecedented sensitivity was achieved exploiting the low background at a level 10^{-4} kg^{-1} keV$_{ee}^{-1}$ day^{-1} in the detector.

DOI: 10.1103/PhysRevLett.113.121301 PACS numbers: 95.35.+d, 12.60.Cn, 14.70.Pw, 14.80.Va

There is overwhelming evidence for the existence of dark matter in the Universe. Since all the evidence is gravitational, the nature of dark matter is not well constrained and various models have been considered. For a model to be falsifiable in a direct detection experiment, it needs to allow at least one interaction beyond the gravitational one. A well motivated model that guides most experimental searches imagines the dark matter particle as a weakly interacting thermal relic, candidates for which are provided by various extensions of the standard model of particle physics. In the case that dark matter is such a weakly interacting massive particle (WIMP), thermal decoupling after the big bang automatically ensures the right relic abundance to account for the observed dark matter. Such a WIMP fits the cold dark matter (CDM) paradigm.

On the other hand, simulations based on this CDM scenario expect a richer structure on galactic scales than those observed. Furthermore, there is so far no evidence of supersymmetric particles at the LHC, and therefore, it is important to investigate various types of dark matter candidates. These facts strengthen an interest to consider lighter and more weakly interacting particles such as super-WIMPs, a warm dark matter candidate [1,2]. If the mass of the super-WIMPs is above ~3 keV, there is no conflict with structure formation in the Universe [3]. Bosonic super-WIMPs are experimentally interesting since their absorption in a target material would deposit an energy essentially equivalent to the super-WIMP's rest mass.

Here, we present direct detection limits obtained with the XMASS-I liquid xenon detector for the vector and the

pseudoscalar case. For the vector super-WIMPs search, this is the first direct detection experiment. The mass range of this study is restricted to 40–120 keV. At the low mass end, we are limited by increasing background, and at high masses, the calculations in Ref. [1] are limited to the mass of the boson less than 100 keV.

The absorption of a vector boson is very similar to the photoelectric effect when the photon energy ω is replaced by the vector boson mass m_V and the coupling constant is scaled appropriately. The cross section, therefore, becomes [1]

$$\frac{\sigma_{\rm abs} v}{\sigma_{\rm photo}(\omega = m_V)c} \approx \frac{\alpha'}{\alpha}, \quad (1)$$

where $\sigma_{\rm abs}$ is the absorption cross section of the vector bosons on an atom, v is the velocity of the incoming vector boson, $\sigma_{\rm photo}$ is the cross section for the photoelectric effect, α is the fine structure constant, and α' is the vector boson analogue to the fine structure constant. For a single atomic species of atomic mass A, the counting rate S_v in the detector becomes [1]

$$S_v \approx \frac{4 \times 10^{23}}{A} \frac{\alpha'}{\alpha} \left(\frac{\rm keV}{m_V}\right) \left(\frac{\sigma_{\rm photo}}{\rm barn}\right) \ {\rm kg}^{-1}\,{\rm day}^{-1}, \quad (2)$$

where the standard local dark matter density of 0.3 GeV/cm^3 [4] is used. Valid ranges for the couplings and masses of thermally produced super-WIMPs are calculated in Refs. [1,2].

The cross section of the axioelectric effect for the pseudoscalar on the other hand is

$$\frac{\sigma_{\rm abs} v}{\sigma_{\rm photo}(\omega = m_a)c} \approx \frac{3m_a^2}{4\pi\alpha f_a^2}, \quad (3)$$

where m_a is the mass of the pseudoscalar particle, and f_a is a dimensionful coupling constant. The counting rate S_a now becomes [1]

$$S_a \approx \frac{1.2 \times 10^{19}}{A} g_{aee}^2 \left(\frac{m_a}{\rm keV}\right) \left(\frac{\sigma_{\rm photo}}{\rm barn}\right) \ {\rm kg}^{-1}\,{\rm day}^{-1}, \quad (4)$$

where $g_{aee} = 2m_e/f_a$, with m_e being the electron mass.

XMASS-I is a large single-phase liquid-xenon detector [5] located underground (2700 m water equivalent) at the Kamioka Observatory in Japan. An active target of 835 kg of liquid xenon is held inside of a pentakis-dodecahedral copper structure that holds 642 inward-looking photomultiplier tubes (PMTs) on its approximately spherical inner surface. The detector is calibrated regularly by inserting ^{57}Co and ^{241}Am sources along the central vertical axis of the detector. Measuring with the ^{57}Co source from the center of the detector volume the photoelectron yield is determined to be 13.9 photoelectrons (p.e.)/keV$_{ee}$ [6], where the subscript ee refers to the customary electron equivalent energy deposit. This large photoelectron yield is realized since the photocathode area covers $> 62\%$ of the inner wall with a large quantum efficiency of $\sim$30% [5]. Data acquisition is triggered if 10 or more PMTs have signals larger than 0.2 p.e. within 200 ns. Each PMT signal is digitized with charge and timing resolution of 0.05 p.e. and 0.4 ns, respectively [7]. The liquid-xenon detector is located at the center of a water Cherenkov veto counter, which is 11 m high and has a 10 m diameter. The veto counter is equipped with seventy-two 50 cm PMTs. Data acquisition for the veto counter is triggered if eight or more of its PMTs register a signal within 200 ns. XMASS-I is the first direct detection dark matter experiment equipped with such an active water Cherenkov shield.

For both, vector and pseudoscalar type super-WIMPs, Monte Carlo (MC) signals are generated by injecting gamma rays uniformly over the entire active volume with a gamma energy corresponding to the rest mass of the boson [8]. This procedure exploits the experimentally relevant aspect that all the energy of a boson including its mass given to an electron is identical to that for gamma rays at these low energies, albeit with different coupling constants in Eqs. (1) and (3).

In the present analysis, we scale the observed number of photoelectrons by 1/13.9 to obtain an event energy E in keV$_{ee}$, without applying the nonlinearity correction of scintillation light efficiency. The MC simulation includes this nonlinearity of the scintillation response [5] as well as corrections derived from the detector calibrations. The absolute energy scale of the MC simulation is adjusted at 122 keV. The systematic difference of the energy scale between data and MC simulation due to imperfect modeling of the nonlinearity in MC simulation is estimated as 3.5% by comparing ^{241}Am data to MC simulation. The decay constants of scintillation light and the timing response of PMTs are modeled to reproduce the time distribution observed with the ^{57}Co (122 keV) and ^{241}Am (60 keV) gamma ray sources [9]. The group velocity of the scintillation light in liquid xenon is calculated from the refractive index ($\sim$11 cm/ns for 175 nm) [10].

Data taken in the commission phase between December 24, 2010 and May 10, 2012 were used for the present analysis. We selected the periods of operation under what we designate normal data taking conditions with a stable temperature (174 ± 1.2 K) and pressure (0.160–0.164 MPa absolute). We have further removed the periods of operation with excessive PMT noise, unstable pedestal levels, or abnormal trigger rates. Total live time is 165.9 day.

Event selection proceeds in four stages that we refer to as cut-1 through cut-4. Cut-1 requires that no outer detector trigger is associated with the events, that they are separated from the nearest event in time by at least 10 ms, and that the rms spread of the inner detector hit timings contributing to the trigger is less than 100 ns. These criteria eliminate

events that are electronics or detector artifacts rather than physical interactions in the detector. Their application reduces the total effective lifetime to 132.0 day in the final sample.

As discussed in Ref. [8,11], the main source of background to the physics analyses stems from surface background, especially the radioactive contaminants in the aluminum seal of the PMTs. We used three additional cuts to reduce those backgrounds. Cut-2 makes use of an event vertex reconstruction. This reconstruction is based on a maximum likelihood evaluation of the observed light distribution in the detector. More detail can be found in Ref. [5]. We select events from the fiducial volume by requiring that the radial distance R of their reconstructed vertex from the center of the detector is smaller than the fiducial volume radius.

The remaining two cuts deal with the issue of misreconstructed events. In particular, radioactive decays on the inner surfaces of the detector pose a problem since light emitted from the flat areas between the PMTs is not necessarily detected by those PMTs surrounding the emission point. Two cuts were developed to identify and eliminate such events. Cut-3 uses the time difference δT_m between the first hit in an event and the mean of the timings of the second half of all the time-ordered hits in the event. Events with smaller δT_m are less likely to be misreconstructed surface events and are kept. Cut-4 eliminates events that reflect their origin within groves or crevices in the inner detector surface through a particular illumination pattern: The rims of the grove or crevice restrict direct light into a disk that is projected as a "band" of higher photon counts onto the inner detector surface. This band is characterized by the ratio $f = (\text{p.e.in a band of width 15 cm})/(\text{total p.e.in the event})$, and F_B is defined by the maximum of f [9]. Events with smaller F_B are less likely to originate from crevices and are selected. Figure 1 shows the distributions of the cut variables described above for ^{57}Co source data and the respective simulations. Similar distributions for ^{241}Am can be seen in Ref. [9]. The reasonable agreement demonstrates the validity of the simulation.

To maximize the sensitivity, cut values are optimized for each super-WIMP mass using its respective super-WIMP MC simulation. The optimization was done by maximizing the ratio of the number of expected signal events to the number of observed background events just outside the signal range. The signal window is ± 15 keV$_{ee}$ around the nominal masses $m_b = m_V$ or m_a shifted according to the energy scale based on MC simulation where the nonlinearity of the scintillation yield is taken into account. Independent of the mass value this signal window contains at least 99% of the signal. For details see Table I. The number of observed background event is counted in the energy range inside $m_b \pm 60$ keV$_{ee}$ but outside $m_b \pm 20$ keV$_{ee}$. To avoid too small of an acceptance, the range of cut values of cut-2 was restricted in the optimization process to be larger than 15 cm. Table I summarizes the resulting cut values. In this table, the efficiency for each cut to retain signals is also shown. These efficiencies were calculated by taking the ratio between the number of generated signal events inside a 15 cm sphere and the number of remaining events after the reduction. The MC events were produced through the entire active volume of the detector.

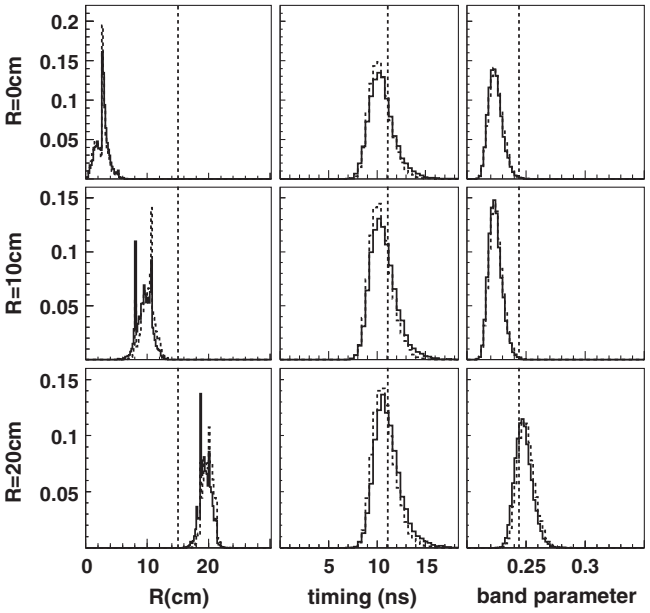

FIG. 1. Comparisons of 122 keV gamma ray data (solid histograms) with simulation (dashed histograms) at three positions in the detector, $R = 0$, 10, and 20 cm, from the top to bottom rows. From left to right, distributions for R, δT_m, and F_B are shown (see the text). Data and simulation are in reasonable agreement. The vertical dashed lines show the cut values for 120 keV.

Figure 2 shows data and simulated signal after applying all the cuts, with the cuts optimized as described in the previous section. No significant excess was seen in the data. The remaining events stem mostly from the radon daughter ^{214}Pb. The amount of radon was estimated by the observed rate of ^{214}Bi-^{214}Po consecutive decays and amounts to 8.2 ± 0.5 mBq [5]. On the basis of this rate, we evaluated the expected number of events in the signal window (see Table I). This number is consistent with the expectation except for the 40 keV case, where some leakage events caused by the radioactivity on the inner surface may not have been rejected. Since such background contributions are less certain, we did not subtract such background when deriving upper limits.

Most of the systematic error taken into account arises from uncertainty in our cut efficiencies. We have used ^{241}Am data for $m_b = 40$, 60, and 80 keV and ^{57}Co data for $m_b = 100$ and 120 keV, where the comparison between data and MC simulation is necessary. For cut-1, systematic errors are negligible. In cut-2, uncertainty for the

TABLE I. Optimized cuts for several cases of m_b. Columns R, δT_m, and F_B list the chosen cut values. For events with R, δT_m, and F_B those smaller than corresponding cut values are kept. Column E shows the range of the signal window in keV$_{ee}$ units. Signal efficiencies ("Eff.(%) column") are obtained from the detector simulation, by taking the ratio between the number of events in the hatched histogram in Fig. 2 and the number of events generated in the fiducial mass, 41 kg, inside the radius of 15 cm of the detector. The "Obs." column shows the number of observed events within the signal window. The last two columns show the resulting constraints on α'/α and g_{aee} at 90% C.L.

m_b (keV)	R (cm)	δT_m (ns)	F_B	E (keV$_{ee}$)	Eff. (%)	Obs.	^{214}Pb expected	α'/α	g_{aee}
40	< 15	< 12.62	< 0.258	23.7–53.7	51 ± 13	48	7.9 ± 0.7	8.0×10^{-26}	1.3×10^{-12}
60	< 15	< 12.54	< 0.248	46.9–76.9	63 ± 16	12	11.6 ± 1.0	6.8×10^{-26}	8.0×10^{-13}
80	< 15	< 11.51	< 0.246	68.1–98.1	59 ± 18	8	9.6 ± 0.8	1.6×10^{-25}	9.2×10^{-13}
100	< 15	< 11.14	< 0.244	89–119	65 ± 20	15	11.4 ± 1.0	6.0×10^{-25}	1.4×10^{-12}
120	< 15	< 11.11	< 0.244	111–141	74 ± 23	18	14.4 ± 1.1	1.2×10^{-24}	1.7×10^{-12}

reconstructed radius was estimated to be ± 1 cm by comparing the reconstructed vertex positions for data and simulation. In changing the radius cut by ± 1 cm, the resulting change in cut efficiency ranges from $\pm 13\%$ to $\pm 17\%$, depending on m_b. For cut-3, the systematic uncertainties were evaluated from the difference in acceptance between data and simulation and the systematic uncertainty in modeling the scintillation decay constants as a function of energy (± 1.5 ns). The resulting systematic uncertainties for cut-3 range from $\pm 12\%$ to $\pm 19\%$. For cut-4, we take the difference in acceptance between data and simulation ($\pm 5\%$). For the final event selection using the ± 15 keV$_{ee}$ signal window, the majority of the systematic uncertainty comes from the energy scale ($\pm 12\%$) and resolution ($\pm 5\%$). Particularly, the scale uncertainty comes from the nonlinearity of the scintillation yield ($\pm 3.5\%$), position dependence ($\pm 2\%$), and time variation ($\pm 3\%$). All these systematic errors are used in the evaluation of the detection efficiency uncertainty listed in Table I.

Dividing the number of events observed by the efficiency evaluated, we derive a 90% confidence level (C.L.) upper limit on the number of bosons absorbed in the fiducial volume without subtracting background evaluated. In this calculation, statistical and systematic uncertainties are added in quadrature. Equations (2) and (4) were used to translate this result into an upper limit on the respective coupling constants, α'/α or g_{aee}. This result is given in Table I and shown in Fig. 3. This is the first direct search for vector bosonic super-WIMPs in this mass range. In this range, the present result excludes the possibility for such WIMPs to constitute all of dark matter. As can be seen in the figure, the obtained limit also is comparable to or better than the current astrophysical constraints. For pseudoscalar super-WIMPs coupling, the present limit improves significantly on previous results [12–16]. This significant improvement was achieved exploiting the low background in the detector at a level of 10^{-4} kg^{-1} keV$_{ee}^{-1}$ day^{-1}, unprecedented in this energy range.

In summary, we searched in XMASS-I for signatures of bosonic super-WIMPs. In 165.9 day of data with an effective live time of 132.0 day in a fiducial mass of 41 kg, no significant signal was observed and stringent limits on the electron coupling of bosonic super-WIMPs with masses in the 40–120 keV range were obtained. For vector bosons, the present experimental limit excludes the possibility that vector super-WIMPs constitute all the dark matter. The absence of the signal also provides the most stringent direct

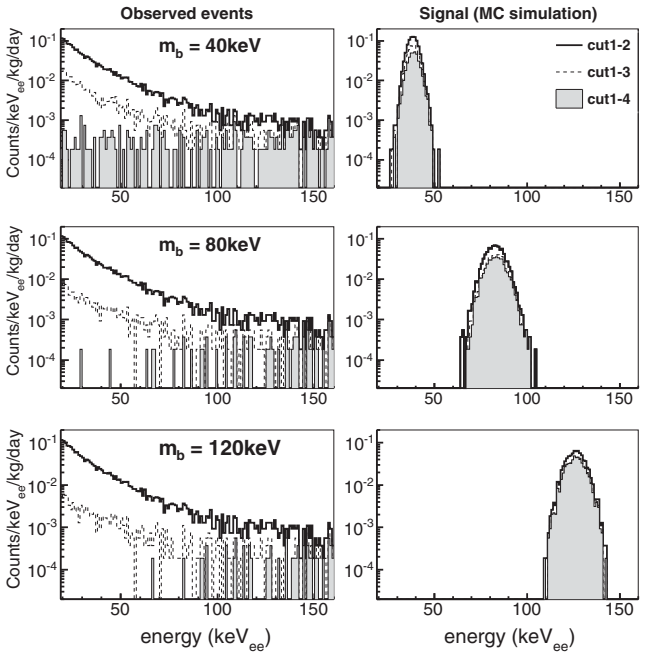

FIG. 2. Energy distribution of the observed events (left column) and simulated events (right column) remaining after each step of the cuts optimized for each vector boson mass individually. From top to bottom, $m_b = 40$, 80, and 120 keV, respectively. In each figure, three histograms are showing events after the cumulative cuts 1–2 (solid line), cuts 1–3 (dashed line), and cut 1–4 (hatched histogram). The effective live time is 132.0 day, and the target mass is 41 kg. The small number of events at the low-energy region in the final samples is due to lower efficiency of cut-4. Efficiencies can be found in Table I. For the simulated events, the dashed line (cuts 1–3) and hatched histogram (cuts 1–4) are barely separated. The coupling constants α'/α assumed in the simulation for 40, 80, and 120 keV are 2.0×10^{-24}, 2.7×10^{-23}, and 1.3×10^{-22}, respectively.

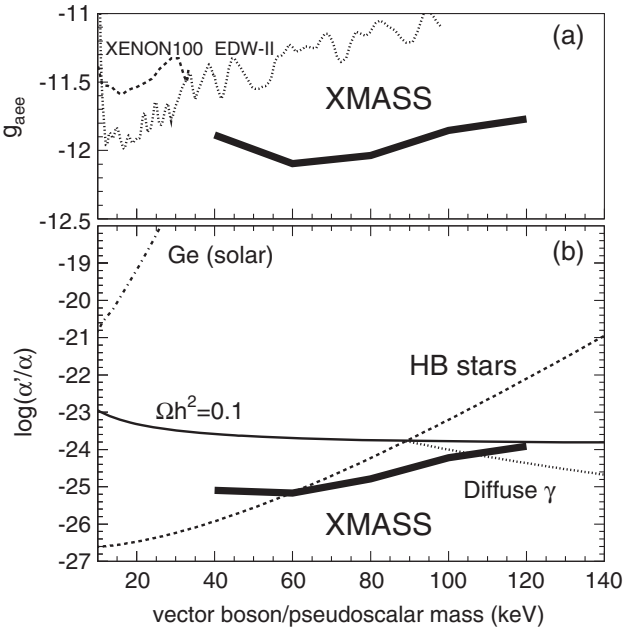

FIG. 3. Limits on coupling constants for (a) electrons and pseudoscalar bosons and (b) electrons and vector bosons at 90% C.L. (thick solid line). (a) Dotted line and dashed line correspond to constraints obtained by EDELWEISS-II [15] and XENON100 [16]. (b) The thin solid line corresponds to the coupling constant required to reproduce the observed dark matter abundance including resonance effects [1,2]. The dotted line and dashed line correspond to the upper limit from the γ ray background from 3γ decays in the Galaxy and the constraint from the He-burning lifetime in horizontal branch (HB) stars, respectively [2]. The dash-dotted line shows an experimental constraint assuming production in the Sun [17].

constraint on the coupling constant of pseudoscalar dark matter to electrons.

We thank Naoki Yoshida for useful discussion on warm dark matter. We gratefully acknowledge the cooperation of the Kamioka Mining and Smelting Company. This work was supported by the Japanese Ministry of Education, Culture, Sports, Science and Technology, Grant-in-Aid for Scientific Research, JSPS KAKENHI Grant No. 19GS0204, and partially by the National Research Foundation of Korea Grant funded by the Korean Government (NRF-2011-220-C00006).

[1] M. Pospelov, A. Ritz, and M. Voloshin, Phys. Rev. D **78**, 115012 (2008).
[2] J. Redondo and M. Postma, J. Cosmol. Astropart. Phys. 02 (2009) 005.
[3] K. Markovič and M. Viel, Pub. Astron. Soc. Aust. **31**, e006 (2014).
[4] J. Beringer *et al.* (Particle Data Group), Phys. Rev. D **86**, 010001 (2012).
[5] K. Abe *et al.* (XMASS Collaboration), Nucl. Instrum. Methods Phys. Res., Sect. A **716**, 78 (2013).
[6] This photoelectron yield is smaller than the value reported in Refs. [5,8,11] since we changed a correction on the charge observed in the electronics. This correction is within the uncertainty reported earlier, ± 1.2 p.e./keV.
[7] S. Fukuda *et al.* (Super-Kamiokande Collaboration), Nucl. Instrum. Methods Phys. Res., Sect. A **501**, 418 (2003).
[8] K. Abe *et al.* (XMASS Collaboration), Phys. Lett. B **724**, 46 (2013).
[9] H. Uchida *et al.* (XMASS Collaboration), Prog. Theor. Exp. Phys. 063C01 (2014).
[10] S. Nakamura (private communication).
[11] K. Abe *et al.* (XMASS Collaboration), Phys. Lett. B **719**, 78 (2013).
[12] R. Bernabei *et al.* (DAMA Collaboration), Int. J. Mod. Phys. A **21**, 1445 (2006).
[13] Z. Ahmed *et al.* (CDMS Collaboration), Phys. Rev. Lett. **103**, 141802 (2009).
[14] C. E. Aalseth *et al.* (CoGeNT Collaboration), Phys. Rev. Lett. **101**, 251301 (2008).
[15] E. Armengaud *et al.* (EDELWEISS-II Collaboration), J. Cosmol. Astropart. Phys. 11 (2013) 067.
[16] E. Aprile *et al.* (XENON100 Collaboration), arXiv: 1404.1455.
[17] R. Horvat, D. Kekez, M. Krčmar, Z. Krečak, and A. Ljubičić, Phys. Lett. B **721**, 220 (2013).